PHYSICAL REVIEW C **95**, 021304(R) (2017)

# Exotic neutron-rich medium-mass nuclei with realistic nuclear forces

Naofumi Tsunoda,[1] Takaharu Otsuka,[1,2,3,4] Noritaka Shimizu,[1] Morten Hjorth-Jensen,[5,6] Kazuo Takayanagi,[7] and Toshio Suzuki[8]

[1]*Center for Nuclear Study, the University of Tokyo, 7-3-1 Hongo, Bunkyo-ku, Tokyo, Japan*
[2]*Department of Physics and Center for Nuclear Study, the University of Tokyo, 7-3-1 Hongo, Bunkyo-ku, Tokyo, Japan*
[3]*National Superconducting Cyclotron Laboratory, Michigan State University, East Lansing, Michigan, 48824, USA*
[4]*Instituut voor Kern- en Stralingsfysica, Katholieke Universiteit Leuven, B-3001 Leuven, Belgium*
[5]*National Superconducting Cyclotron Laboratory and Department of Physics and Astronomy, Michigan State University, East Lansing, Michigan, 48824, USA*
[6]*Department of Physics, University of Oslo, N-0316 Oslo, Norway*
[7]*Department of Physics, Sophia University, 7-1 Kioi-cho, Chiyoda-ku, Tokyo 102, Japan*
[8]*Department of Physics, College of Humanities and Sciences, Nihon University, Sakurajosui 3, Setagaya-ku, Tokyo 156-8550, Japan*

(Received 14 January 2016; revised manuscript received 23 January 2017; published 17 February 2017)

We present the first application of the newly developed extended Kuo-Krenciglowa (EKK) theory of the effective nucleon-nucleon interaction to shell-model studies of exotic nuclei, including those where conventional approaches with fitted interactions encounter difficulties. This EKK theory enables us to derive an interaction that is suitable for several major shells ($sd + pf$ in this work). By using such an effective interaction obtained from the Entem-Machleidt QCD-based $\chi$N$^3$LO interaction and the Fujita-Miyazawa three-body force, the energies, $E2$ properties, and spectroscopic factors of low-lying states of neutron-rich Ne, Mg, and Si isotopes are nicely described, as the first shell-model description of the "island of inversion" without fit of the interaction. The long-standing question as to how particle-hole excitations occur across the $sd$-$pf$ magic gap is clarified with distinct differences from the conventional approaches. The shell evolution is shown to appear similarly to earlier studies.

DOI: 10.1103/PhysRevC.95.021304

*Introduction.* The nuclear shell model [1,2] provides a unified and successful description of both stable and exotic nuclei, as a many-body framework which can be related directly to nuclear forces. Exotic nuclei are located far from the $\beta$-stability line on the Segrè chart, exhibiting very short life times, mainly due to an unbalanced ratio of proton ($Z$) and neutron ($N$) numbers. Exotic nuclei differ remarkably in some other aspects from their stable counterparts, providing us with new insights into understanding atomic nuclei and nuclear forces [3–5]. As experimental data on exotic nuclei are, in general, less abundant than data on stable nuclei, theoretical calculations, interpretations, and predictions play an ever increasing role.

Shell-model (SM) calculations handle the nuclear forces in terms of two-body matrix elements (TBMEs). In the early days, TBMEs were empirically determined in order to reproduce certain observables. A well-known example is the effective interaction for $p$-shell nuclei by Cohen and Kurath [6]. A breakthrough toward more microscopically derived TBMEs was achieved by Kuo and Brown for $sd$-shell nuclei [7]. Although the basic features of the nucleon-nucleon ($NN$) force for the SM calculation are included in these effective interactions, empirical adjustments of TBMEs were needed in order to reproduce various observables [8–10].

These effective interactions were all derived for a Hilbert space represented by the degrees of freedom of one major (oscillator) shell. As we move toward exotic nuclei, some new features and phenomena arise. A notable example can be the shell evolution due to nuclear forces between a proton and a neutron in different shells [5,11,12]. This leads to significant particle-hole excitations between two shells, for example, in $Z = 8$–14 neutron-rich exotic nuclei [3–5,9,11–17]. A microscopic understanding of many of these phenomena requires the degrees of freedom of at least two major shells.

Deriving SM effective Hamiltonians is a challenge to nuclear theory. Several attempts have been made recently in this direction [18–24], while the issue of two major shells is still unsettled.

The aim of this work is first to derive a SM interaction for the model space consisting of the $sd$ and $pf$ shells based on the so-called extended Kuo-Krenciglowa (EKK) method [25–27]. Second, we apply this interaction to our studies of exotic neutron-rich Ne, Mg, and Si isotopes. These are nuclei in and around the so-called island of inversion [14], where the degrees of freedom of $sd$ and $pf$ shells are essential. We thus present, in this Rapid Communication, the first application of the EKK method to actual cases. Three-nucleon forces (3NFs) are also included since they play an important role in reproducing basic nuclear properties [28–32].

*Hamiltonian and model spaces.* Many-body perturbation theory (MBPT) has been the method of choice for deriving effective interactions for the nuclear shell model; see for example Refs. [33–37]. The conventional MBPTs, for instance, the Kuo-Krenciglowa (KK) method [33–35], are constructed for degenerate single-particle states in the model space, which usually refers to one major shell [33–37]. The present model space, however, includes all single-particle states of the $sd$ and the $pf$ shells, labeled $sdpf$ hereafter. This leads to possible divergences when constructing an effective interaction with conventional MBPTs due to the nondegeneracies of the

 

single-particle states. A practical, but not satisfactory, way to circumvent such divergences has been to enforce in an *ad hoc* manner the degenerate single-particle energies for all involved single-particle states spanning a model space; see for example Refs. [29,38,39]. Employing the EKK method as done in this work removes the above-mentioned divergence problems and allows a correct treatment of the different single-particle energies [27]. Starting from a Hamiltonian which contains kinetic energy and a two-body $NN$ interaction and following the formalism described in Ref. [27], we can define an effective Hamiltonian through

$$H_{\rm eff} = H_{\rm BH}(\xi) + \sum_{k=1}^{\infty} \frac{1}{k!} \frac{d^k \hat{Q}(\xi)}{d\xi^k} \{H_{\rm eff} - \xi\}^k, \qquad (1)$$

where $H_{\rm BH}$ and $\hat{Q}$ are the Bloch-Horowitz Hamiltonian and the so-called $\hat{Q}$-box [36,37], respectively. The latter contains only linked and unfolded Feynman-Goldstone diagrams in MBPT. The quantity $\xi$ is a parameter (the origin of the $\hat{Q}$-box expansion), and the poles of $\hat{Q}(\xi)$ can be avoided with appropriate value.

We renormalize the $NN$ interaction using the so-called $V_{{\rm low}k}$ approach with a cutoff of 2.0 fm$^{-1}$ [40–42]. We solve Eq. (1) with a harmonic oscillator basis with the oscillator parameter $\hbar\omega = 45A^{-1/3}$–$25A^{-2/3}$ MeV $= 12.10$ MeV where $A = 28$ ($A = Z + N$). The $\hat{Q}$-box is calculated up to the third order in Eq. (1) and intermediate excitations up to $17\,\hbar\omega$ are included to guarantee convergence in the sum over intermediate states. Three-nucleon forces are included through the Fujita-Miyazawa term with its strength given by a standard $\pi$-$N$-$\Delta$ coupling [43]. This term is in turn transformed into a medium-dependent two-body interaction; see Refs. [28,39,44] for details.

The single-particle energies (SPEs) in the $sdpf$ space are input too. Because of on-going efforts toward a better description of density profiles [32], which is directly related to the size of the shell gap, we employ here $^{16}$O as the closed-shell core and fit the values of SPEs to selected observables such as ground-state energies of $N < 20$, $^{34}$Si $2^+_1$ level, etc. The energies of the $2p_{1/2}$ and the $1f_{5/2}$ orbits are constrained by the GXPF1 Hamiltonian of Ref. [10], due to a lack of appropriate data. These SPEs, i.e., one-body part of the Hamiltonian, will be confirmed to be reasonable, because effective SPEs to be calculated for $Z = N = 20$ will turn out close to SPEs known for $^{40}$Ca. The SPEs are isospin invariant because of the $^{16}$O core.

In this work we study Ne ($Z = 10$), Mg ($Z = 12$), and Si ($Z = 14$) isotopes with a focus on $N \sim 20$ nuclei. Eigenvalues and eigenstates are obtained via the standard Lanczos diagonalization method, including up to 8-particle–8-hole (8p8h) excitations from the $sd$ shell to the $pf$ shell. For the cases where the Lanczos diagonalization is infeasible (e.g., $N > 22$) because of too large dimension, we switch to a Monte Carlo SM calculation [45,46].

The TBMEs vary gradually as a function of $A$ because $\hbar\omega$ changes. Although TBMEs can be calculated for each nucleus explicitly, we introduce an overall scaling factor $(A/A_0)^{-0.2}$ with $A_0 = 28$. The value of the power is determined so that TBMEs calculated explicitly for several nuclei can be best reproduced by this simple parametrization.

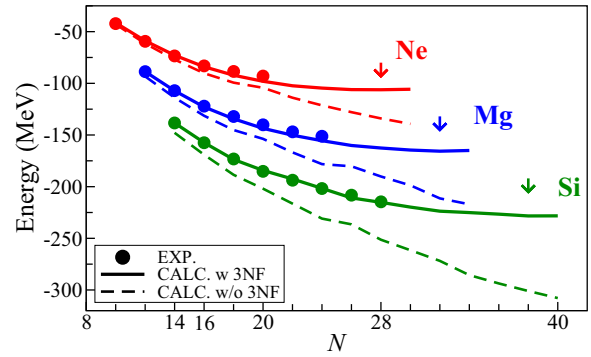


FIG. 1. Ground-state energies of Ne, Mg, and Si isotopes. Experimental values are compared against shell-model results with and without 3NF. Arrows indicate the predicted drip lines. Experimental data are taken from Ref. [47].

*Results and discussions.* Figure 1 shows the experimental ground-state energies (Coulomb-force effects subtracted) of Ne, Mg, and Si isotopes compared with our theoretical calculations with and without three-body forces.

Figure 1 indicates that the ground-state energies are well reproduced when 3NF effects are included. It is also worth noticing that the repulsion due to the 3NF grows as $N$ increases in all the isotopic chains. This is consistent with earlier studies [28,39]. We point out that this repulsion becomes stronger also as $Z$ increases, suggesting that the present 3NF contribution is repulsive also in the proton-neutron channel. Figure 1 shows also present predictions for the drip lines [48,49].

Figure 2(a) shows the $2^+$ and $4^+$ energy levels. Experimental levels are well reproduced by the present calculation, including both gradual and steep changes as a function of $N$. For instance, the $2^+_1$ level drops down steeply by $\sim$1 MeV from $N = 16$ to 18 in the Ne chain, while a similar change occurs from $N = 18$ to 20 in the Mg chain. The $4^+_1$ levels show a different behavior as functions of $N$. For instance, in Mg isotopes, from $N = 16$ to 18, it starts to come down whereas the $2^+_1$ level stays constant, implying that not only the degree of deformation but also the shape is changing. On the other hand, in Si isotopes, the $2^+_1$ level jumps up at $N = 20$. These behaviors of excited levels are reproduced well by the present calculation. The low excitation energy of the $2^+_1$ levels in $^{30}$Ne and $^{32}$Mg indicates that these nuclei are strongly deformed and that $sd$-to-$pf$ particle-hole (ph) excitations over the $N = 20$ gap occur significantly. In contrast, the higher lying $2^+_1$ level of $^{34}$Si suggests weaker degrees of ph excitations.

Figure 2(b) shows $B(E2 : 0^+_1 \rightarrow 2^+_1)$ values. With effective charges, $(e_p, e_n) = (1.25, 0.25)e$, calculated $B(E2)$ values exhibit systematic behaviors in agreement with experiment. This agreement is, however, not as good as that obtained for the energy levels. This probably indicates the need to derive the $E2$ operator using the same microscopic theory. While the $N = 20$ shell closure in Si isotopes is evident also in $B(E2)$ systematics, the $B(E2)$ values of Ne and Mg isotopes are larger

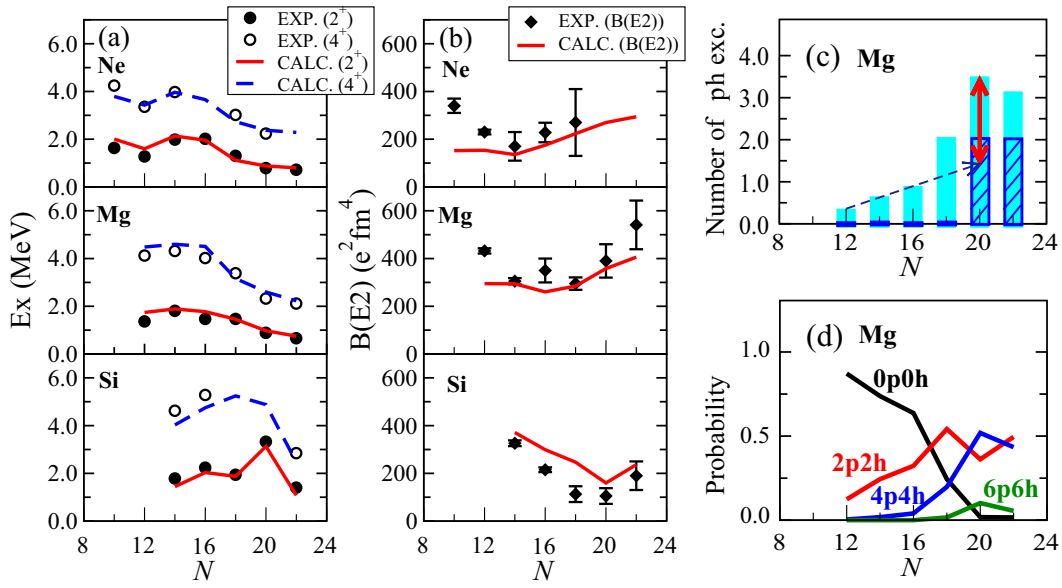


FIG. 2. (a) Excitation energies of first $2^+$ and $4^+$ states and (b) $B(E2:0_1^+ \to 2_1^+)$ values of Ne, Mg, and Si isotopes. Experimental data [47,50] and present calculations are compared. (c) Expectation values of the number of the particle-hole excitations in the ground state of Mg isotopes. The plain histograms are present results, while the hatched ones imply the value by [14]. The dashed line shows the trend. The two-way arrow indicates the additional 2p2h excitation (see the text). (d) Decomposition of ph-excitation probabilities for the ground state of Mg isotopes.

at $N = 20$ than at $N = 18$, a feature which is consistent with the growing deformation seen in the $2_1^+$ level.

Regarding higher spin states, Fig. 3 shows, as an example, yrast levels of $^{32}$Mg, of which the $6^+$ level was measured recently by Crawford *et al.* [51]. The present result is in agreement with observed levels as well as those calculated by the sdpf-U-mix interaction [17]. The calculated $B(E2; J^+ \to (J-2)^+)$ values are 70, 96, 36, and 58, ($e^2$ fm$^4$) for $J = 2,4,6$, and 8, respectively. We note that the $6^+$ and $8^+$ members of the yrast band are mixed with less deformed states in the present calculation, reducing their energies and $B(E2)$ values from the rotor systematics.

We now turn to properties of the wave functions of Mg isotopes. Figure 2(c) depicts the expectation value of the number of ph excitations over the $Z = N = 20$ shell gap for the ground state. One notices the abrupt increase at

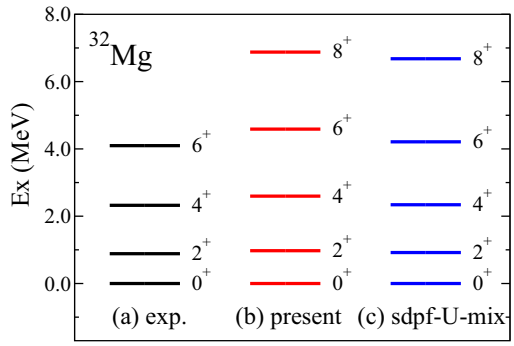


FIG. 3. Yrast levels of $^{32}$Mg obtained by (a) experiment [51], (b) present work, and (c) calculation with the sdpf-U-mix interaction [17,51].

$N = 18$ and furthermore at $N = 20$. These increases are associated with the onset of large deformation. More particles (predominantly neutrons) in the *pf* shell and many holes in the *sd* shell enhance collective motion toward more deformed nuclear shapes. The average value of the ph excitations is about 3.5 for $^{32}$Mg. This is a large number, compared to the conventional picture for $^{32}$Mg being basically a 2p2h state [9,14–17]. The value assumed in the Warburton-Becker-Brown island-of-inversion model [14] is shown in Fig. 2(c) as a reference. The basic trend remains unchanged in other shell-model calculations, although the actual values can be somewhat larger [9,15–17].

In the present calculation, this ph value starts low (<0.5) at $N = 12$, and increases almost monotonically to $N = 16$. This increase is a "modest" effect of the effective interaction shifting nucleons between the two shells, e.g., pairing effects. Considering that the $2_1^+$ level remains high (∼2 MeV) up to $N = 18$, this ph excitation mode does not produce a strong deformation. We extrapolate it linearly up to $N = 20$ in Fig. 2(c). The difference between the extrapolated and actual values is about 2, which can be interpreted as an additional 2p2h excitation essential for promoting the strong deformation. Although this interpretation is intuitive, the 2p2h excitation on top of the "modest" correlation appears to be analogous to the 2p2h picture seen in the conventional approaches.

Figure 2(d) shows more details of the ph excitations involved in the Mg ground states. The probability of the 0p0h configuration comes down slowly for $N \leqslant 16$, and drops down sharply after that. The 2p2h probability increases gradually until $N = 16$. The 4p4h is negligible up to $N = 16$, but increases abruptly for $N \geqslant 18$, especially for $N = 20$. Note that the 2p2h probability even decreases at $N = 20$. Such

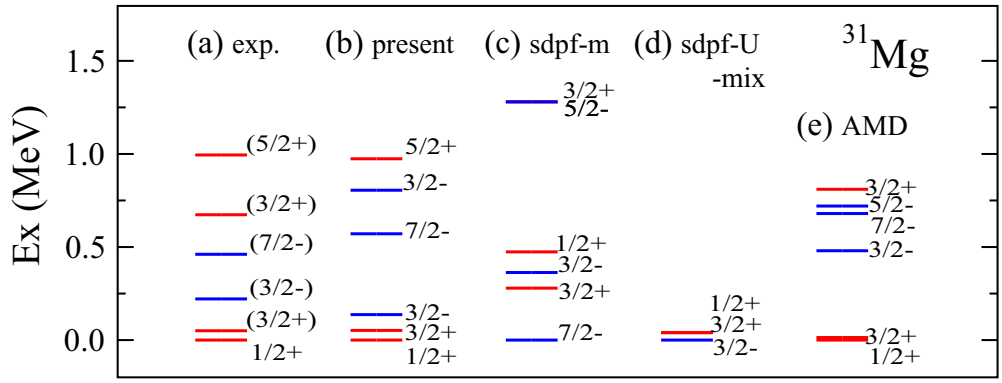


FIG. 4. Energy levels of $^{31}$Mg. (a) experimental values, (b) present work, (c) sdpf-m [16], (d) sdpf-U-mix [17], and (e) AMD+GCM calculation [52].

changes drive the nucleus toward stronger deformation by including higher ph configurations. The present work thus resolves, for the first time, the long-standing question as to how the *sd*-to-*pf* excitation grows from stable to exotic Mg isotopes, showing notable differences from conventional approaches.

In constructing effective $NN$ interactions for the *sd* shell, e.g., USD [8], certain effects of *sd*-*pf* ph excitations are renormalized into TBMEs within the *sd* shell. If an *sd*-*pf* interaction is constructed on top of this *sd*-shell interaction (with minor changes), a renormalized fraction of those excitations should not appear explicitly. In fact, this is the case with the *sdpf*-*m* interaction (probably as well as others), with the above-mentioned expectation value being as small as 0.05, 0.08, 0.20, 0.85, 2.25, and 1.96 for $^{24-34}$Mg, respectively. In some cases, however, the explicit treatment of those excitations becomes crucial.

For transitional nuclei around $^{32}$Mg, the mixing of different ph configurations is indeed crucial since the deformations contribute less to its binding energy. We show low-lying positive- and negative-parity levels of $^{31}$Mg in Fig. 4. The present calculation reproduces the experimental levels rather well, for example, in the ordering of the lowest four levels. The configurations of the positive-party states are of 0p0h (normal) by 1–3%, 2p2h by 66–68%, and 4p4h by 29–30%. In contrast, the lowest $3/2^-$ and $7/2^-$ states consist of 33–35% 1p1h (normal), 55–57% 3p3h, and 11% 5p5h configurations. Thus, the ph properties differ significantly between positive- and negative-parity states, whereas similar ph excitations can be found within the same parity. It is clear that the coupling between different ph configurations has to be evaluated precisely. Figure 4 includes the results of other calculations. Among them, only the shell-model calculation of [17] reproduces the near-degeneracy of the three lowest levels. Further fits of TBMEs were not attempted in Ref. [17]. This is natural because of too many parameters with two major shells. The present work, however, generates all TBMEs from first principles thanks to the EKK method, and no further fine-tuning of the effective interaction is done.

We briefly discuss a test of the present wave functions by transfer reactions. The spectroscopic factors are calculated as 0.77 and 1.41 for one-neutron removal from $^{32}$Mg ground state to $3/2^-_1$ and $7/2^-_1$ states, respectively. The experimental values are 0.59(11) and 1.19(36) [53], respectively, which are in good agreement after scaling the theoretical values by the usual quenching factor ∼0.7 [54,55]. Thus, the present wave functions, which look different from those of conventional calculations, turn out to be quite consistent with these experimental values.

The last primary subject is the effective single-particle energy (ESPE). The ESPE represents the combined effect on the single-particle energies from the inert core and the monopole effects from other valence nucleons, producing important effects on the shell structure of exotic nuclei [5,11,12,28]. Figure 5 shows the neutron ESPEs of the $N = 20$ isotones, calculated in the normal filling scheme, with and without 3NF and tensor force component. Here the tensor force component is extracted from a spin-tensor decomposition of the present $NN$ effective interaction generated by the EKK method [27]. Figure 5(a) indicates that the primary effect of 3NF is to raise all orbits by similar amounts [28]. Without 3NF effect, the neutron orbits are bound too deeply, yielding excessive binding energies, as seen in Fig. 1. On the other hand, Fig. 5(b) demonstrates that the tensor force lowers or raises the ESPEs depending on the cases, and thereby changes rather rapidly the spacing between certain orbits [11]. The ESPEs obtained at $N = 20$, including other *sd*-*pf* orbits, appear to

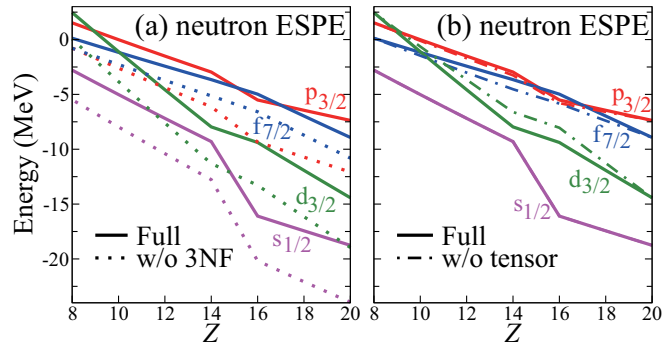


FIG. 5. ESPEs of $N = 20$ isotones for neutrons obtained in the normal filling scheme. (a) The case with and without three-nucleon forces. (b) The case with and without the tensor force.

be reasonable for $^{40}$Ca, suggesting the validity of the input SPEs being used.

Figures 5(a) and 5(b) indicate that the neutron $sd$-$pf$ gap grows rapidly as $Z$ increases from $Z = 8$ to $Z = 14$, and stays relatively constant after $Z = 14$ up to $Z = 20$ as being the $N = 20$ magic gap. This gap, however, disappears around $Z = 8$, and the $N = 16$ magic gap arises instead [56–58]. This is consistent with the trend shown by the simplified interaction, called the monopole-based universal interaction $V_{\rm MU}$ [12], where the central force gives a steady enlargement of the gap from $Z = 8$ to $Z = 20$, while the tensor force makes the change more rapid for $Z < 14$ but cancels the change for $Z > 14$. The neutron ESPEs of $f_{7/2}$ and $p_{3/2}$ at $Z = 20$ are also consistent with those from empirically determined interactions [16]. Two other upper orbitals, $p_{1/2}$ and $f_{5/2}$ appear at the energies similar to those of another empirical interaction [10], although not shown in Fig. 5. We thus demonstrate, for the first time, what type of shell evolution a chiral $NN$ interaction such as the $\chi$N$^3$LO interaction produces in medium-mass exotic nuclei. It is seen also that the lowering as a function of $Z$ is dampened by three-nucleon forces. The resulting trend is similar to that obtained with the $V_{\rm MU}$ interaction of Ref. [12] as well as other interactions fitted to experiment [9,16,17].

*Summary.* We have presented a consistent microscopic description of neutron-rich nuclei $Z = 10$–$14$ and $N \sim 20$ employing the EKK method to derive appropriate multishell effective interactions. The calculated energies, $B(E2)$ values, and spectroscopic factors are in good agreement with experiment. Our TBMEs are not fitted and the quality of the agreement is similar to or better than SM approaches with fitted TBMEs. Definite differences from conventional approaches are seen, particularly in the pattern of particle-hole excitations between the $sd$ and $pf$ shells. In this context, the conventional 2p2h picture of the island of inversion serves as an intuitive interpretation. We point out that the above-mentioned differences can be smaller if ph excitations over the relevant magic gap are included explicitly in the fit of TBMEs, as in the case for the $pf + 1g_{9/2}$ orbit, e.g., [59,60]. The shell evolution is derived from the chiral EFT force and Fujita-Miyazawa three-body force for the first time. All these features will contribute to further studies of exotic nuclei where microscopic theories play crucial roles. Further progress in nuclear forces and many-body treatments will improve the agreement to experiment and provide us with more predictive power.

Recently, Macchiavelli *et al.* reported [61] that the ground state of $^{32}$Mg is dominated by 2p2h and 4p4h configurations with nearly equal probabilities. Although this result was obtained in an empirical analysis by a one-parameter mixing of three $0^+$ states and the structure of $^{30}$Mg taken in [61] differs from the present one, it is of interest that such large probabilities were obtained in both works independently.

*Acknowledgments.* We thank Dr. Y. Utsuno for useful discussions. The Lanczos shell-model calculation is performed with the code KSHELL [62]. This work was supported in part by Grants-in-Aid for Scientific Research (23244049, 15K05090), by the HPCI Strategic Program (hp140210, hp150224, hp160221), by MEXT and JICFuS as a priority issue (elucidation of the fundamental laws and evolution of the universe) to be tackled by using the Post "K" Computer, and by the CNS-RIKEN joint project for large-scale nuclear structure calculations. M.H.J. acknowledges U.S. NSF Grant No. PHY-1404159 (Michigan State University) and the Research Council of Norway under Contract No. ISP-Fysikk/216699.

[1] M. Mayer, Phys. Rev. **75**, 1969 (1949).
[2] O. Haxel, J. H. D. Jensen, and H. E. Suess, Phys. Rev. **75**, 1766 (1949).
[3] O. Sorlin and M. G. Porquet, Prog. Part. Nucl. Phys. **61**, 602 (2008).
[4] A. Gade and T. Glasmacher, Prog. Part. Nucl. Phys. **60**, 161 (2008).
[5] T. Otsuka, Phys. Scr. **T152**, 014007 (2013).
[6] S. Cohen and D. Kurath, Nucl. Phys. **73**, 1 (1965).
[7] T. T. S. Kuo and G. E. Brown, Nucl. Phys. **85**, 40 (1966).
[8] B. A. Brown, W. A. Richter, R. E. Julies, and B. H. Wildenthal, Ann. Phys. (NY) **182**, 191 (1988).
[9] E. Caurier, G. Martínez-Pinedo, F. Nowacki, A. Poves, and A. P. Zuker, Rev. Mod. Phys. **77**, 427 (2005).
[10] M. Honma, T. Otsuka, B. A. Brown, and T. Mizusaki, Phys. Rev. C **65**, 061301 (2002).
[11] T. Otsuka, T. Suzuki, R. Fujimoto, H. Grawe, and Y. Akaishi, Phys. Rev. Lett. **95**, 232502 (2005).
[12] T. Otsuka, T. Suzuki, M. Honma, Y. Utsuno, N. Tsunoda, K. Tsukiyama, and M. Hjorth-Jensen, Phys. Rev. Lett. **104**, 012501 (2010).
[13] X. Campi, H. Flocard, A. K. Kerman, and S. Koonin, Nucl. Phys. A **251**, 193 (1975).
[14] E. K. Warburton, J. A. Becker, and B. A. Brown, Phys. Rev. C **41**, 1147 (1990).
[15] N. Fukunishi, T. Otsuka, and T. Sebe, Phys. Lett. B **296**, 279 (1992).
[16] Y. Utsuno, T. Otsuka, T. Mizusaki, and M. Honma, Phys. Rev. C **60**, 054315 (1999).
[17] E. Caurier, F. Nowacki, and A. Poves, Phys. Rev. C **90**, 014302 (2014).
[18] A. F. Lisetskiy, B. R. Barrett, M. K. G. Kruse, P. Navrátil, I. Stetcu, and J. P. Vary, Phys. Rev. C **78**, 044302 (2008).
[19] S. K. Bogner, H. Hergert, J. D. Holt, A. Schwenk, S. Binder, A. Calci, J. Langhammer, and R. Roth, Phys. Rev. Lett. **113**, 142501 (2014).
[20] G. R. Jansen, J. Engel, G. Hagen, P. Navrátil, and A. Signoracci, Phys. Rev. Lett. **113**, 142502 (2014).
[21] L. Coraggio, A. Covello, A. Gargano, and N. Itaco, Phys. Rev. C **87**, 034309 (2013).
[22] L. Coraggio, A. Covello, A. Gargano, and N. Itaco, Phys. Rev. C **89**, 024319 (2014).
[23] J. Simonis, K. Hebeler, J. D. Holt, J. Menéndez, and A. Schwenk, Phys. Rev. C **93**, 011302(R) (2016).
[24] G. R. Jansen, M. D. Schuster, A. Signoracci, G. Hagen, and P. Navratil, Phys. Rev. C **94**, 011301 (2016).

[25] K. Takayanagi, Nucl. Phys. A **852**, 61 (2011).
[26] K. Takayanagi, Nucl. Phys. A **864**, 91 (2011).
[27] N. Tsunoda, K. Takayanagi, M. Hjorth-Jensen, and T. Otsuka, Phys. Rev. C **89**, 024313 (2014).
[28] T. Otsuka, T. Suzuki, J. D. Holt, A. Schwenk, and Y. Akaishi, Phys. Rev. Lett. **105**, 032501 (2010).
[29] J. D. Holt, T. Otsuka, A. Schwenk, and T. Suzuki, J. Phys. G **39**, 085111 (2012).
[30] G. Hagen, M. Hjorth-Jensen, G. R. Jansen, R. Machleidt, and T. Papenbrock, Phys. Rev. Lett. **108**, 242501 (2012).
[31] G. Hagen, M. Hjorth-Jensen, G. R. Jansen, R. Machleidt, and T. Papenbrock, Phys. Rev. Lett. **109**, 032502 (2012).
[32] A. Ekström, G. R. Jansen, K. A. Wendt, G. Hagen, T. Papenbrock, B. D. Carlsson, C. Forssén, M. Hjorth-Jensen, P. Navrátil, and W. Nazarewicz, Phys. Rev. C **91**, 051301 (2015).
[33] T. T. S. Kuo, S. Y. Lee, and K. F. Ratcliff, Nucl. Phys. A **176**, 65 (1971).
[34] E. M. Krenciglowa and T. T. S. Kuo, Nucl. Phys. A **235**, 171 (1974).
[35] E. M. Krenciglowa, T. T. S. Kuo, E. Osnes, and P. J. Ellis, Nucl. Phys. A **289**, 381 (1977).
[36] T. Kuo and E. Osnes, Lect. Notes Phys. **364**, 1 (1990).
[37] M. Hjorth-Jensen, T. T. S. Kuo, and E. Osnes, Phys. Rep. **261**, 125 (1995).
[38] J. D. Holt, J. Menéndez, and A. Schwenk, Phys. Rev. Lett. **110**, 022502 (2013).
[39] J. D. Holt, J. Menéndez, J. Simonis, and A. Schwenk, Phys. Rev. C **90**, 024312 (2014).
[40] D. R. Entem and R. Machleidt, Phys. Rev. C **68**, 041001 (2003).
[41] S. Bogner, T. T. S. Kuo, L. Coraggio, A. Covello, and N. Itaco, Phys. Rev. C **65**, 051301 (2002).
[42] A. Nogga, S. K. Bogner, and A. Schwenk, Phys. Rev. C **70**, 061002 (2004).
[43] A. M. Green, Rep. Prog. Phys. **39**, 1109 (1976).
[44] J. D. Holt, J. Menéndez, and A. Schwenk, Eur. Phys. J. A **49**, 39 (2013).
[45] T. Otsuka, M. Honma, T. Mizusaki, N. Shimizu, and Y. Utsuno, Prog. Part. Nucl. Phys. **47**, 319 (2001).
[46] N. Shimizu, T. Abe, Y. Tsunoda, Y. Utsuno, T. Yoshida, T. Mizusaki, M. Honma, and T. Otsuka, Prog. Theor. Exp. Phys. **2012**, 1A205 (2012).
[47] NuDat (Nuclear Structure and Decay Data), http://www.nndc.bnl.gov/nudat2/.
[48] H. Koura, T. Tachibana, M. Uno, and M. Yamada, Prog. Theor. Phys. **113**, 305 (2005).
[49] J. Erler, N. Birge, M. Kortelainen, W. Nazarewicz, E. Olsen, A. M. Perhac, and M. Stoitsov, Nature **486**, 509 (2012).
[50] S. Takeuchi, M. Matsushita, N. Aoi, P. Doornenbal, K. Li, T. Motobayashi, H. Scheit, D. Steppenbeck, H. Wang, H. Baba *et al.*, Phys. Rev. Lett. **109**, 182501 (2012).
[51] H. L. Crawford, P. Fallon, A. O. Macchiavelli, A. Poves, V. M. Bader, D. Bazin, M. Bowry, C. M. Campbell, M. P. Carpenter, R. M. Clark *et al.*, Phys. Rev. C **93**, 031303 (2016).
[52] M. Kimura, Phys. Rev. C **75**, 041302 (2007).
[53] J. R. Terry, B. A. Brown, C. M. Campbell, J. M. Cook, A. D. Davies, D. C. Dinca, A. Gade, T. Glasmacher, P. G. Hansen, B. M. Sherrill *et al.*, Phys. Rev. C **77**, 014316 (2008).
[54] A. Gade, P. Adrich, D. Bazin, M. D. Bowen, B. A. Brown, C. M. Campbell, J. M. Cook, T. Glasmacher, P. G. Hansen, K. Hosier *et al.*, Phys. Rev. C **77**, 044306 (2008).
[55] J. A. Tostevin and A. Gade, Phys. Rev. C **90**, 057602 (2014).
[56] B. A. Brown, Revista Mexicana de Fisica **39**, Suppl. 2, 21 (1993).
[57] A. Ozawa, T. Kobayashi, T. Suzuki, K. Yoshida, and I. Tanihata, Phys. Rev. Lett. **84**, 5493 (2000).
[58] T. Otsuka, R. Fujimoto, Y. Utsuno, B. A. Brown, M. Honma, and T. Mizusaki, Phys. Rev. Lett. **87**, 082502 (2001).
[59] M. Honma, T. Otsuka, T. Mizusaki, and M. Hjorth-Jensen, Phys. Rev. C **80**, 064323 (2009).
[60] Y. Tsunoda, T. Otsuka, N. Shimizu, M. Honma, and Y. Utsuno, Phys. Rev. C **89**, 031301 (2014).
[61] A. O. Macchiavelli, H. L. Crawford, C. M. Campbell, R. M. Clark, M. Cromaz, P. Fallon, M. D. Jones, I. Y. Lee, M. Salathe, B. A. Brown *et al.*, Phys. Rev. C **94**, 051303 (2016).
[62] N. Shimizu, arXiv:1310.5431v1.